AIAS 2019 International Conference on Stress Analysis

Error analysis in the determination of the dynamic coefficients of tilting pad journal bearings

M. Barsanti[a], E. Ciulli[a], P. Forte[a,*], M. Libraschi[b], M. Strambi[c]

[a]*Department of Civil and Industrial Engineering, University of Pisa, Largo Lazzarino, 56122 Pisa, Italy*
[b]*BHGE, Via Felice Matteucci 2, 50127 Florence, Italy*
[c]*AM Testing, Via Padre Eugenio Barsanti 10, Loc. Ospedaletto, 56121 Pisa, Italy*

Abstract

In this work, a method for the determination of the systematic error affecting the computation of dynamic coefficients of Tilting Pad Journal Bearings (TPJB) is described. This statistical method is applied to the coefficients obtained for a 5-pad TPJB with 280 mm diameter. Experimental activity was carried out on an advanced experimental test rig specifically designed for investigations on large size high-performance bearings for turbomachinery. The adopted configuration has the test article (TA) floating at the center of a rotor supported by two rolling bearings. The TA is statically loaded by a hydraulic actuator and excited by two orthogonal hydraulic actuators with a single tone or multitone dynamic load. The linear coefficient computation method is based on the dynamic measurement of forces, accelerations and relative displacements of rotor and bearing. The analysis of the acquired data is carried out in the frequency domain, after signal Fast Fourier Transform (FFT) computation. Along with a description of the experimental setup and of the main characteristics of the sensors used for data acquisition, this paper presents a statistical technique for the estimation of the systematic error and a comparison with the random error.

1. Introduction

The characteristics of bearings strongly influence rotordynamic behaviour. Therefore the determination of the bearing stiffness and damping coefficients is quite important. This is usually done experimentally, applying dynamic loads to the rotor or the bearing and measuring their relative displacement. Computational techniques, mainly in the frequency domain, based on dynamical models are then used for the determination of the stiffness and damping coefficients.

---

* Paola Forte Tel.: +39-050-221-8046 ; fax: +39-050-221-0604.
  E-mail address: paola.forte@unipi.it

An uncertainty analysis must be carried out to validate the experimental results, to increase the validity of comparisons of results from different labs or processes, to provide a reliable tool for quality assurance of measurements and research results, as stated by Wells (1992). In the literature, the experimentally determined bearing dynamic characteristics are reported with their uncertainty interval, usually with 95 confidence, referring to the guidelines of ANSI/ASME PTC 19.1 (2019) and ISO GUM (2008) standards. Fundamental is also the paper by Moffat (1998) who describes the sources of errors in engineering measurements, the relationship between error and uncertainty and the procedure of an uncertainty analysis from the identification of the intended true value of a measurement to the estimation of the individual errors and interpretation of the results and reporting. The errors associated with a measurement process are fixed (bias or systematic) errors and random (precision) errors. Errors may arise from calibration, data acquisition, and data reduction each with bias and precision components, as stated in ANSI/ASME PTC 19.1 (2019). Errors in measurements of various parameters (e.g. forces, displacements, mass, acceleration) are propagated into derived results (e.g. bearing dynamic coefficients). Few papers give details about the adopted technique to perform such an analysis on the results of the journal bearing dynamic coefficient identification. A procedure for the evaluation of the systematic errors that considers also uncertainties on masses and on shaft geometrical dimensions is described by Salazar and Santos (2016).

A novel experimental apparatus has been set up by the Department of Civil and Industrial Engineering of the University of Pisa in collaboration with BH TPS and AM Testing. With such an apparatus, bearings can be statically and dynamically characterized varying their peripheral speeds, the static and dynamic loads (single tone or multitone). Several sensors allow the simultaneous measurements of significant quantities to highlight the characteristics of the test bearing and monitor the condition of the test facility. This work reports the results of the first static and dynamic tests on a 5-pad high-performance tilting pad journal bearing, focusing on the analysis of errors affecting the experimental results and in particular the identification of dynamic coefficients. In particular, a methodology to estimate their systematic uncertainty is proposed. In the last section, the systematic uncertainty is compared to the random one.

2. Experimental activity

The test rig employed in this work is described in detail in the papers by Forte et al. (2016, 2018) and Ciulli et al. (2018). A longitudinal section of the test cell, that is part of the test rig with the TPJB, is shown in figure 1. The rig was specifically designed to study the dynamical properties of large size high-performance bearings for turbomachinery, typically 4- or 5-pad TPJB. Its characteristics are briefly described below. Bearings with diameters from 150 mm to 300 mm and bearing length to diameter ratio from 0.4 to 1 can be tested. A configuration with a floating test bearing housing at the centre of a rotor supported by two rolling bearings is adopted. The bearing oil flow rate can be varied from 125 to 1100 l/min and the oil inlet temperature from 30 to 120 °C. The plant maximum total required power is 1 MW.
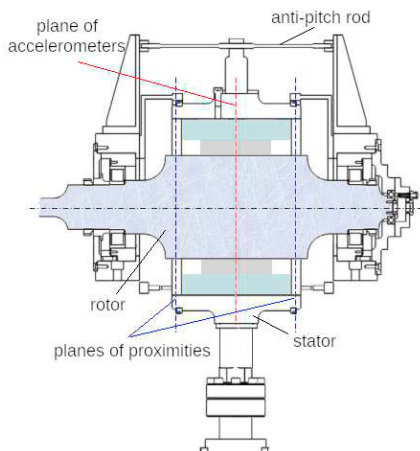

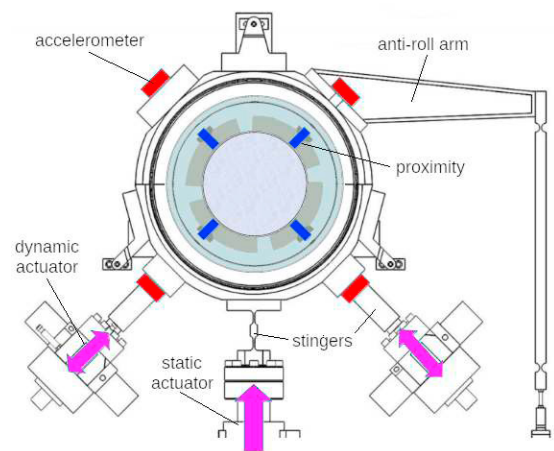Fig. 1. Longitudinal section of the test cell evidencing sensor planes.

Fig. 2. Cross section of the test cell evidencing actuators and sensors.

The rotor is driven by a 630 kW electric motor connected to a gearbox with a transmission ratio of 6, so that the shaft rotational speed can be varied from about 500 to 24000 rpm. In the test described in this work, the shaft rotational speed varied in the range 1000-7500 rpm. Static and dynamic loads are applied to the bearing case by three hydraulic actuators, as shown in Figure 2. The static actuator can apply a maximum load of 270 kN upwards. The dynamic actuators (each one at 45° compared to the vertical direction) can work one at a time or simultaneously, in the latter case producing a vertical force when operating with equal amplitude in phase, and a horizontal force when operating in antiphase. The dynamic load is obtained summing up to five sinusoidal excitations (tones) individually adjustable in terms of amplitude and frequency. The maximum frequency of the dynamic load is 350 Hz, its maximum amplitude is 40 kN.

A load cell with 300 kN full-scale is located between the static actuator and the bearing case. Two instrumented stingers, inserted between the dynamic actuators and the bearing case, act as triaxial load cells (with 5 kN full-scale on two axes and 40 kN on the third one) for the dynamical measurement of all the significant force components.

Eight proximity sensors, with a precision of about 0.1 μm and a measuring range of 2000 μm, are placed on two parallel planes perpendicular to the bearing axis for measuring the relative displacements of the bearing housing and the rotor along with the directions of the dynamic actuators.

Four accelerometers with a typical sensitivity of 20 mV/g (at 159 Hz, 10.0 g rms) measure the stator acceleration at the mid-section, in the direction of the dynamic actuators.

Tests are managed by a very complex control and data acquisition system. About 30 high-frequency signals are usually sampled at 50 kHz while about 60 low-frequency signals are sampled at 1 Hz.

3. Dynamic coefficients computation technique

The dynamic coefficient computation technique is reported here for completeness. The dynamic stiffness and damping coefficients are computed using the data acquired during two tests with linearly independent excitations for each excitation angular frequency ω. In-phase and anti-phase operating modes of the dynamic actuators are used for obtaining the two datasets which are the input for the computational procedure. The FFT of the signals is used for the identification process of the dynamic coefficients. Taking advantage of linearity when a multi-tone test is performed, the FFT allows the determination of forces, displacements and accelerations components at each of the excitation frequencies. For each of the excitation frequencies the following calculation procedure is followed. The first step consists in the determination of the net bearing film force by subtracting the stator inertia force from the forces applied to the stator which are measured by the load cell-instrumented stingers in the frequency domain, as shown in eq. (1).

$$\begin{bmatrix} F_{b1x} & F_{b2x} \\ F_{b1y} & F_{b2y} \end{bmatrix} = \begin{bmatrix} F_{s1x} & F_{s2x} \\ F_{s1y} & F_{s2y} \end{bmatrix} - M \begin{bmatrix} A_{1x} & A_{2x} \\ A_{1y} & A_{2y} \end{bmatrix} \tag{1}$$

F indicates the amplitude of the force FFT, A the amplitude of the acceleration FFT, M the stator mass, while for the subscripts b and s refer to bearing and stator respectively, x and y refer to the horizontal and vertical direction respectively, 1 and 2 to the anti-phase and in-phase test respectively.

In the second step, a linear model is adopted to relate the net bearing film forces to the corresponding displacements by the so called bearing impedance matrix H, as it is shown in eq. (2).

$$\begin{bmatrix} F_{b1x} & F_{b2x} \\ F_{b1y} & F_{b2y} \end{bmatrix} = \begin{bmatrix} H_{xx} & H_{xy} \\ H_{yx} & H_{yy} \end{bmatrix} \begin{bmatrix} X_1 & X_2 \\ Y_1 & Y_2 \end{bmatrix} \tag{2}$$

Then the (complex) elements H_{ij} of the impedance matrix H can be determined, in the frequency domain, using the classical methodology described by Al-Ghasem and Childs (2005), simply by multiplying the [2×2] force complex matrix by the corresponding inverse displacement complex matrix, as shown in eq. (3).

$$\begin{bmatrix} H_{xx} & H_{xy} \\ H_{yx} & H_{yy} \end{bmatrix} = \begin{bmatrix} F_{b1x} & F_{b2x} \\ F_{b1y} & F_{b2y} \end{bmatrix} \begin{bmatrix} X_1 & X_2 \\ Y_1 & Y_2 \end{bmatrix}^{-1} \tag{3}$$

where X, Y indicate the amplitudes of the displacement transform for anti-phase (subscript 1) and in-phase (subscript 2) tests. The stiffness k and damping c coefficients are finally obtained as respectively the real and the imaginary parts of the impedance direct and cross-coupled coefficients:

$$\begin{bmatrix} H_{xx} & H_{xy} \\ H_{yx} & H_{yy} \end{bmatrix} = \begin{bmatrix} k_{xx} & k_{xy} \\ k_{yx} & k_{yy} \end{bmatrix} + i\omega \begin{bmatrix} c_{xx} & c_{xy} \\ c_{yx} & c_{yy} \end{bmatrix} \tag{4}$$

For each operating condition, 30 samples of forces and displacements have been acquired, each obtained by computing the FFT of the signals on a 3 s time window. The mean values of the dynamic coefficients are finally computed averaging a sample of impedance matrices obtained in the same operating conditions. Once the coefficients are calculated at all the excitation frequencies, the synchronous dynamic coefficients can be obtained by interpolation at the rotational frequency.

In this work, a technique is proposed for the evaluation of the systematic errors on the estimated mean values of the dynamic coefficient. The systematic uncertainty is eventually compared with the random error. The calibration of the experimental apparatus is assumed to be affected by random errors during the calibration setup. Instruments and devices used for the calibration procedure are assumed to be perfectly calibrated. Other parameters needed to build the data set, such as the statoric mass M, are considered to be exactly known.

4. Determination of calibration uncertaintes of the sensors

This work analyzes the calibration method of 8 proximity sensors (measurements of Xs), 7 force sensors (measurements of Fs) and 4 accelerometers (measurements of As). The voltage output signals must therefore be converted in three different physical quantities. The starting points for the conversion procedure are the data reported in the calibration sheets attached to each of the sensors. For each of the sensors, a linear calibration model is used, thus assuming to have relations of the following type

$$F = m_F \cdot V_F + q_F \qquad X = m_X \cdot V_X + q_X \qquad A = m_A \cdot V_A \tag{5}$$

In the accelerometer calibration technique used by the manufacturer, the frequency of the sample acceleration is varied keeping its amplitude constant. Only the sensitivities (as a function of the excitation frequencies) are reported. Therefore it is not possible to estimate the value of an eventual intercept q_A. For the other sensors, the constant terms q_F and q_X have been evaluated even if, using the FFT of the signal in the following analysis, their contributions are inessential.

Therefore, the key point is the estimation of the best value of the angular coefficients m_F, m_X, m_A and their dispersion. For the analysis carried out in the present work, the calibration coefficients declared in the calibration sheets were taken as reference values for these angular coefficients, which were then also used to obtain the reference values of the dynamic coefficients. In the following, it will be clear that this choice does not influence too much the evaluation of systematic error, the main objective of this work. Concerning the range of variation of the angular coefficients, the following methods were used.

1) For the accelerometers, the extremes of the calibration coefficient in the working frequency range were used to determine the width of a uniform distribution centred around the reference value of the calibration coefficient.

2) For the proxy sensors, the reproducibility of the positions during the calibration process was indicated in the calibration sheet, therefore the positions have been assumed to have a gaussian distribution with standard deviation estimated as half the reproducibility. The precision of the digital voltage meter was reported to be 0.1 mV. As the reported least significant digit was at the mV level without any associated uncertainty, the voltage was supposed to be precisely measured at this level and the measured voltage values were assumed to be uniformly distributed with a width of 0.5 mV. These values were used for an estimation of the calibration coefficient distribution using a least-squares linear fit technique together with a random generation of calibration data.

3) For the load cells, the standard error on parameters obtained after a least-squares linear fit was used as standard deviations for gaussian distributions of the generated random calibrations.

An example of the results, for one of the load cells, is shown in Figure 3.

Using this technique, 200 independent artificial calibrations, all consistent with the dispersion of the data acquired in the calibration procedure reported in the calibration sheets, were generated for each of the sensors.
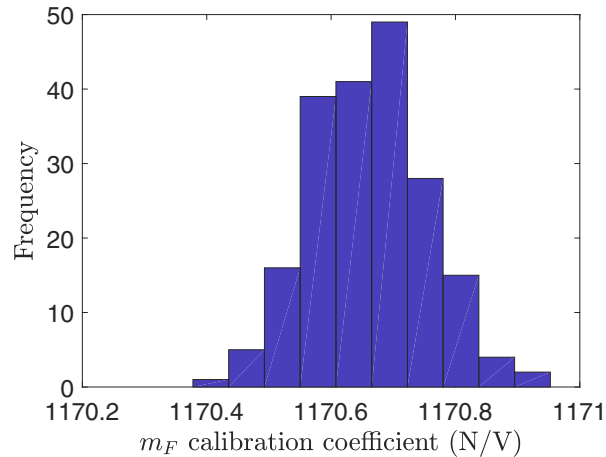
Fig. 3. An example of frequency distribution of the calibration coefficient for one of the load cells.

5. Computation of systematic error

The raw voltage signals were converted to the quantities to be measured using the artificial calibration obtained using the procedure described in section 4. As a result, 200 different data samples were obtained, each of which can be considered as a possible experimental result in agreement with the calibration procedure described in the calibration sheets. Each of the data samples was used for dynamical coefficient computation following the method reported in section 3. In this way, $200 \times 30 = 6000$ values of stiffness coefficients were obtained for each operating condition and for each excitation frequency. Each of these values was compared with what was considered the best estimate of the corresponding coefficient that was computed using the reference calibration. In this way, even if the reference calibration were wrong, evaluation of the data dispersion would be anyway reliable. The amplitudes of these dispersions are a measure of the systematic errors, that is to say of the uncertainties that are associated to errors that are still present after calibration, even if the calibration procedure is assumed correct and performed using perfectly calibrated instruments. It is reasonable that the dispersions do not depend too much from the reference calibration. Therefore the difference of the extremes of the bilateral 95% confidence intervals, empirically obtained taking the 151th and the 5880th element of the sorted dataset, has been taken as twice the amplitude of the systematic error. This choice allows an easier comparison with the random error, as it will be shown later. An example of distribution of the deviations for one of the stiffness coefficients is reported in Figure 4.

The computation of the confidence intervals for the various dynamic coefficients has been repeated for each operating condition and for each excitation frequency. The results can be superimposed as error bars to the estimated values of the dynamic coefficients themselves, similarly to the representation of random errors. The only difference is that the possible deviation of the values due to random errors computed at different excitation frequencies are not correlated, while the deviations due to systematic error are roughly the same. To evidence this difference, the bars are reported using dashed lines. The results for stiffness coefficients are reported in Figure 5, for damping coefficients in Figure 6. The various scales on the y−axes are different in each panel, to evidence the range of variation of each dynamic coefficient. It is therefore possible to compare this range with the amplitude of the systematic error bar. It is evident that in all considered cases the range of variation of the stiffness and damping coefficients (as a function of the excitation frequency) is much larger than the amplitude of the systematic error.

It can be immediately noticed that the amplitude of systematic error interval does not depend very much on the excitation frequency. A computation of the sample correlation matrix among the set of the deviations computed at the 5 excitation frequencies shows correlation coefficients higher than 0.99. This means that the broken lines joining the dots in the figures 5 and 6 move rigidly as the calibration changes.
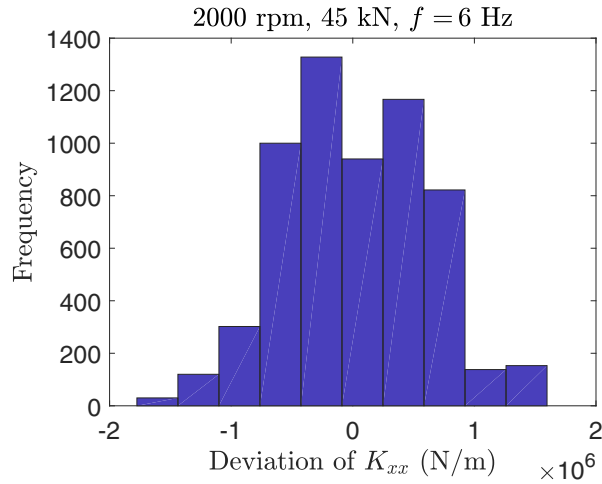
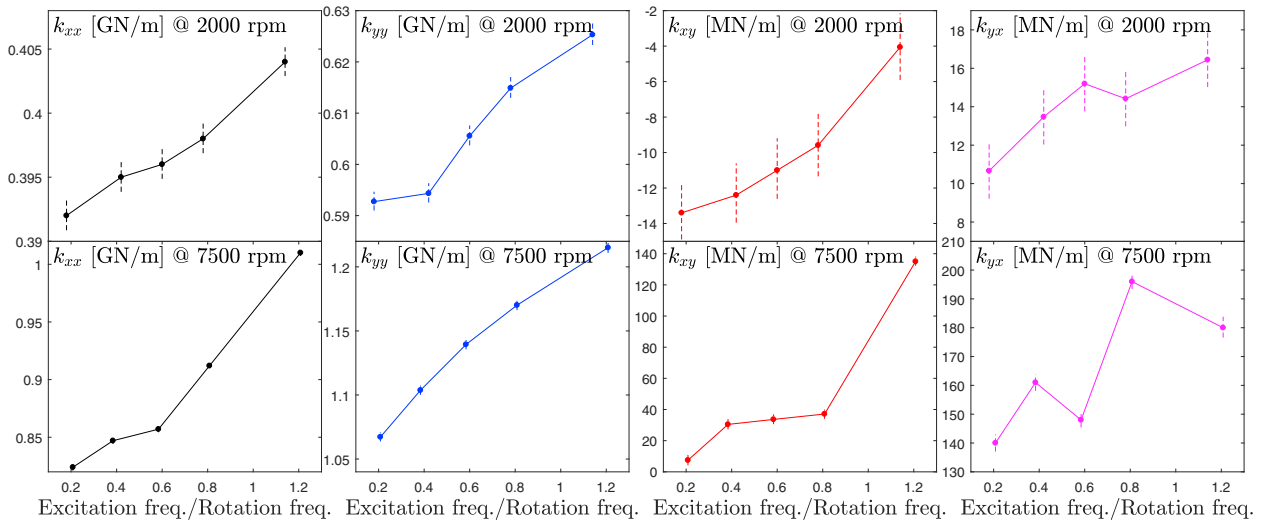Fig. 4. An example of frequency distribution of k_{xx} deviations.

Fig. 5. Stiffness coefficients as a function of the relative excitation frequency for two different shaft rotational speeds. The dashed bar indicates systematic error (interval of deviation from the reference value for 95% of the calibration procedures). Note that the scales are different in each panel to highlight the amplitudes of the systematic error bars with respect to the different ranges of variation of the stiffness coefficients.

6. Comparison of random and systematic errors

A detailed analysis of the random error associated to the estimated dynamic coefficients is reported by Barsanti et al. (2019). The simplest method for random error computation is based on the calculation of the standard deviation of the sample made of 30 values of the dynamic coefficients. Assuming that the Central Limit Theorem holds (that is to say that 30 is a sufficiently high sample numerosity to consider it as infinite), the standard deviation of the estimated dynamic coefficients (averaging the 30 values) is obtained by dividing each sample standard deviation by $\sqrt{30}$. The 95% confidence interval half-width can finally be obtained by multiplying the standard deviation of the mean by 1.96. Barsanti et al. (2019) showed that a more complex methods for the estimate of random error gives substantially the same results. In this section the two types of error are compared reporting the amplitudes of the two sides of the confidence intervals (with respect to each estimated mean value) on the same figure. Both upper and lower extremes are presented, to show that in some cases there is a slight asymmetry for systematic error. This could be due to a slight unbiasing of the method for the systematic error estimation. The results for stiffness coefficients are reported
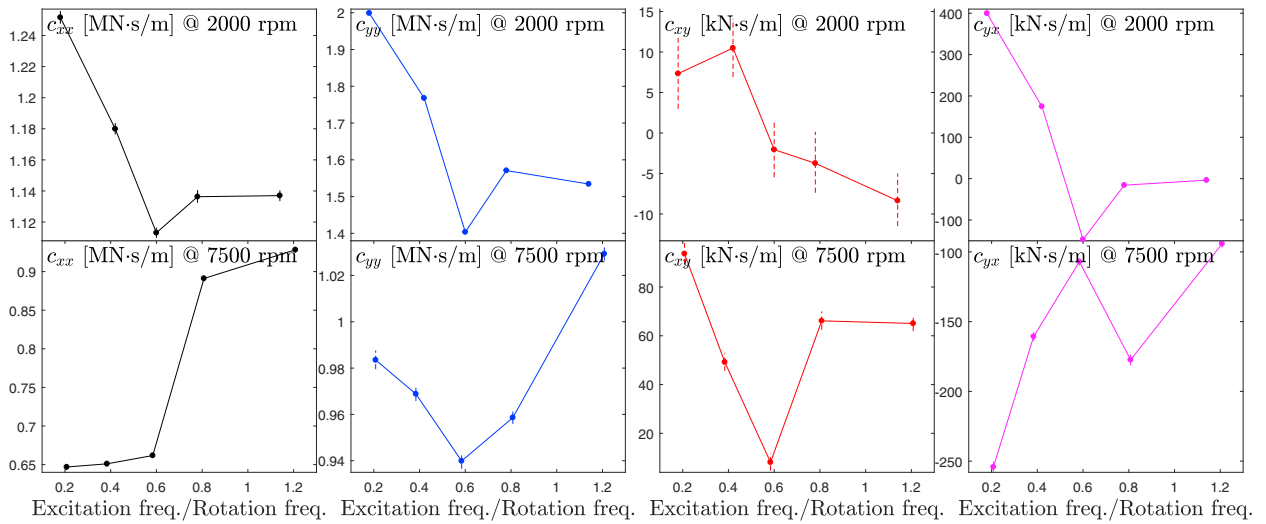
Fig. 6. Damping coefficients as a function of the relative excitation frequency for two different shaft rotational speeds. The dashed bar indicates systematic error (interval of deviation from the reference value for 95% of the calibration procedures). Note that the scales are different in each panel to highlight the amplitudes of the systematic error bars with respect to the different ranges of variation of the damping coefficients.
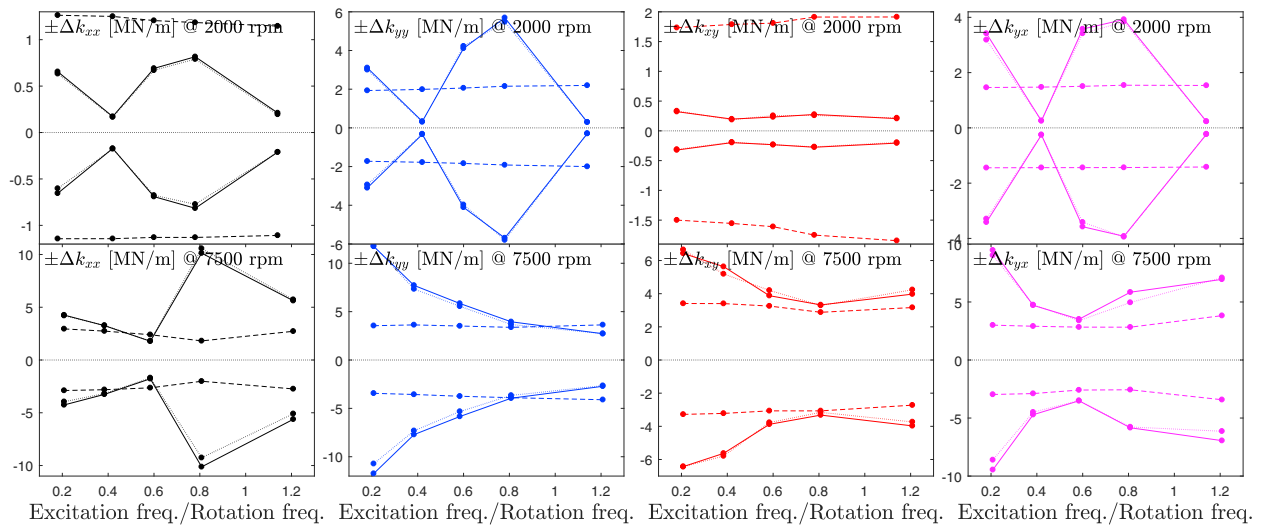

Fig. 7. Comparison of systematic errors (dashed lines) with random error for stiffness coefficients as a function of the relative excitation frequency for two different shaft rotational speeds. Full lines: random uncertainty computed using sample standard deviation. Dotted lines: random uncertainty computed using bootstrap technique, as described by Barsanti et al. (2019).

in figure 7, for damping coefficients in Figure 8. For completeness, random errors computed using both methods are reported. As it can be seen, the full and dotted lines are practically overlapping. Sometimes a slight asymmetry of the bootstrap confidence intervals is observable with respect to the Gaussian ones which are, by definition, symmetrical. This could indicate that the use of the Central Limit Theorem is not entirely justified for this dataset.

A large variety of confidence intervals width is evident for random errors when the excitation frequency is varied. On the contrary, for systematic error the width of confidence intervals does not vary too much when the excitation frequency is changed. Variations of the setup conditions (shaft speed and static load) seem to influence the value of systematic uncertainty, even if its order of magnitude remains the same. The variation of systematic error when setup conditions are changed is lower than the variation of the random uncertainty as a function of the excitation frequency which, in some conditions, can even be of an order of magnitude.
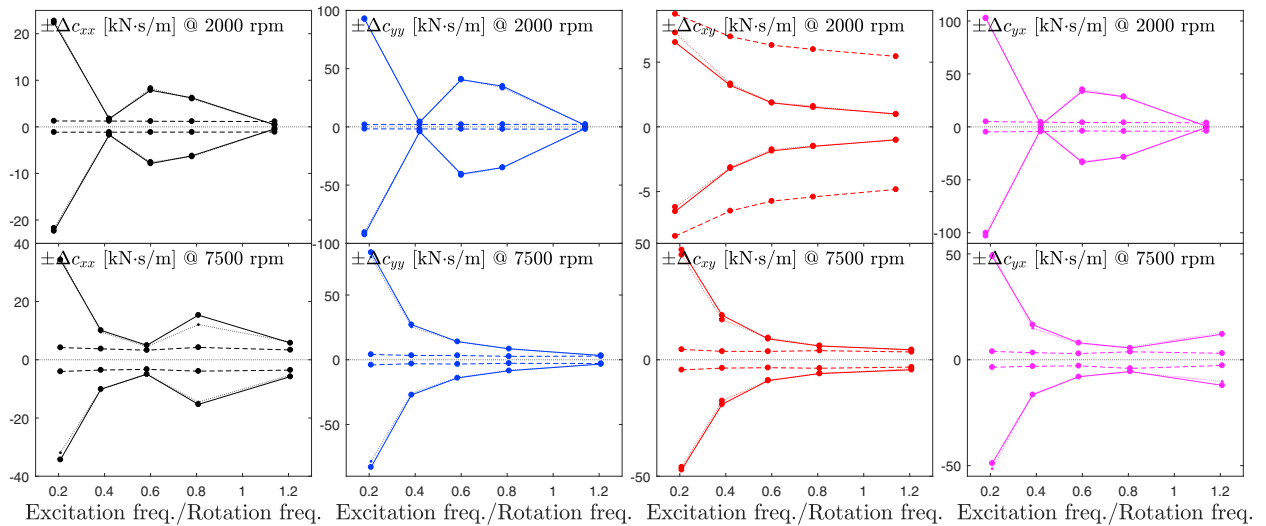
Fig. 8. Comparison of systematic errors (dashed lines) with random error for damping coefficients as a function of the relative excitation frequency for two different shaft rotational speeds. Full lines: random uncertainty computed using sample standard deviation. Dotted lines: random uncertainty computed using bootstrap technique, as described by Barsanti et al. (2019).

7. Conclusions

This paper presented a method for the determination of the systematic error associated to the computation of the dynamic coefficients of a Tilting Pad Journal Bearing. The algorithm computes a set of independent random calibrations which are consistent with the calibration uncertainties reported in the calibration sheets. These calibrations are used to obtain a set of distributions of the bearing stiffness and damping coefficients in various operating conditions. Their mean values are in agreement with the values obtained using the reference calibration, therefore the distribution of the deviations from the reference values are statistically meaningful. Their 95% confidence intervals are reported together with confidence intervals of random errors. The most significant result of this work is that the systematic errors associated with each stiffness or damping coefficient, in the investigated experimental setup, are of the same magnitude order of random uncertainties.

Future development of this study will include an evaluation of the importance of non-linearities both in the sensor response functions and in the dynamic model of the TPJB described by Ciulli and Forte (2019). The importance of higher order coefficients and the variation of first order coefficients due to non-linear effects can be correctly estimated only if it is possible to evaluate the uncertainties associated with these coefficients. Moreover, a study of the critical steps in the calibration procedures could give some useful hints for decreasing the systematic error. Finally, a model for the explanation of the dependance of the random uncertainty on excitation frequency could be of help for a better setup of the experimental conditions.

References

Al-Ghasem, A., Childs, D., 2005. Rotordynamic coefficients measurements versus predictions for a high-speed flexure pivot tilting pad bearing (load-between-pad configuration). ASME Turbo Expo 2005: power for the land, sea, and air June 6-9 Reno Nevada (USA) 4, 725–736.

ANSI/ASME PTC 19.1, 2019. ANSI/ASME PTC-19.1 Test Uncertainty. Technical Report. American Standard of Mechanical Engineers.

Barsanti, M., Ciulli, E., Forte, P., 2019. Random error propagation and uncertainty analysis in the dynamic characterization of Tilting Pad Journal Bearings. Journal of Physics: Conference Series 1264, 012035.

Ciulli, E., Forte, P., 2019. Nonlinear response of tilting pad journal bearings to harmonic excitation. Machines 7, 43–56.

Ciulli, E., Forte, P., Libraschi, M., Nuti, M., 2018. Set-up of a novel test plant for high power turbomachinery tilting pad journal bearings. Tribology International 127, 276–287.

Forte, P., Ciulli, E., Maestrale, F., Nuti, M., Libraschi, M., 2018. Commissioning of a novel test apparatus for the identification of the dynamic coefficients of large tilting pad journal bearings. Procedia Structural Integrity 8, 462–473.

Forte, P., Ciulli, E., Saba, D., 2016. A novel test rig for the dynamic characterization of large size tilting pad journal bearings. Journal of Physics: Conference Series 744, 012159.

ISO GUM, 2008. ISO/IEC Guide 98-3 Uncertainty of measurement – Part 3: Guide to the expression of uncertainty in measurement (GUM:1995). Technical Report. International Organization for Standardization. Geneva, CH.

Moffat, R.J., 1998. Describing the uncertainties in experimental results. Experimental Thermal and Fluid Science 1, 3–17.

Salazar, J.G., Santos, I.F., 2016. Experimental identification of dynamic coefficients of lightly loaded tilting-pad bearings under several lubrication regimes. Proceedings of IMechE Part J: Journal of Engineering Tribology 12, 1423–1438.

Wells, C.V., 1992. Principles and applications of measurement uncertainty analysis in research and calibration. 3rd Annual infrared radiometric sensor calibration symposium September 14-17 Logan Utah (USA) .